Edelweiss Applied Science and Technology
ISSN: 2576-8484
Vol. 8, No. 4, 1387-1401
2024
Publisher: Learning Gate
DOI: 10.55214/25768484.v8i4.1513

Graphene-functionalized photonic crystal fibers for detecting the refractive index of a wide range of analyzes

Farah Salim Neamah[1]*, Hassan A Yasser[1]
[1]Department of Physics, College of Science, University of Thi-Qar, Thi-Qar, Iraq; farah.salim@utq.edu.iq (F.S.N.).

Abstract: This study looks into a new photonic crystal fiber (PCF) sensor covered in graphene that can detect changes in the analyte's refractive index (RI) in the COMSOL environment. The sensor operates by detecting a peak in light loss that varies in wavelength based on the RI of the analyte. Higher RI analytes shift the peak towards longer wavelengths. It is explored how many factors affect the sensor's performance, such as graphene's Fermi energy, the site inside the fiber, and the thickness of the gold layer. The location of graphene and its Fermi energy have a substantial influence on how the sensor responds. Interestingly, the resonant wavelength has a linear relationship with the RI of the analyte, which allows for precise RI calculation. Increasing gold thickness improves light-material interaction, but subsequent thickening has a detrimental impact, lowering sensor sensitivity. The appropriate thickness varies according to the material under consideration. Finally, the analysis determines the optimal arrangement of graphene for maximum sensitivity by completely covering the analyte holes in the PCF. By finding the right balance between these factors, the suggested sensor can have both high spectral sensitivity and low sensor resolution.

Keywords: *PCF, Plasmonic, Sensitivity of sensor.*

1. Introduction

Graphene, a single layer of carbon atoms organized in a honeycomb lattice, has unique features that make it perfect for improving photonic crystal fiber (PCF)-based refractive index (RI) sensors. Graphene's huge surface area enables more contact with the analyte, resulting in a larger signal [1]. The electrical conductivity of graphene may be tuned, allowing researchers to customize the sensor's response to specific analytes. Graphene may sustain surface plasmons, which are collective electron oscillations that are extremely sensitive to changes in the surrounding environment [2]. The surface plasmon resonance (SPR) effect considerably increases the sensor's responsiveness to RI fluctuations [3]. While graphene has various benefits, integrating it into PCFs poses certain challenges: Matching the thermal expansion coefficients of graphene and the surrounding glass fiber is critical for preventing breaking during production [4]. Developing strategies for depositing a homogenous and well-controlled graphene layer on the PCF is critical for achieving constant sensor performance [5]. Researchers are addressing these difficulties in numerous ways, including: This approach enables the controlled development of graphene directly on the PCF surface [6]. Graphene can be generated on a different substrate and then transferred to the PCF [7]. Doping graphene with certain components or functionalizing its surface can help it interact with the desired analyte [8]. Graphene-functionalized PCFs have various benefits over traditional RI sensors: The combination of PCF's light-directing capabilities and graphene's SPR effect produces extremely sensitive RI detection [9, 10]. These sensors have the capacity to detect a wide range of refractive indices, making them useful for a variety of applications [11, 12]. Graphene, a single layer of carbon atoms organized in a honeycomb lattice, has unique features that make it perfect for improving photonic crystal fiber (PCF)-based refractive index

* Correspondence: farah.salim@utq.edu.iq

(RI) sensors. Graphene's huge surface area enables more contact with the analyte, resulting in a larger signal [1]. The electrical conductivity of graphene may be tuned, allowing researchers to customize the sensor's response to specific analytes. Graphene may sustain surface plasmons, which are collective electron oscillations that are extremely sensitive to changes in the surrounding environment [2]. The surface plasmon resonance (SPR) effect considerably increases the sensor's responsiveness to RI fluctuations [3]. While graphene has various benefits, integrating it into PCFs poses certain challenges: Matching the thermal expansion coefficients of graphene and the surrounding glass fiber is critical for preventing breaking during production [4]. Developing strategies for depositing a homogenous and well-controlled graphene layer on the PCF is critical for achieving constant sensor performance [5]. Researchers are addressing these difficulties in numerous ways, including: This approach enables the controlled development of graphene directly on the PCF surface [6]. Graphene can be generated on a different substrate and then transferred to the PCF [7]. Doping graphene with certain components or functionalizing its surface can help it interact with the desired analyte [8]. Graphene-functionalized PCFs have various benefits over traditional RI sensors. The combination of PCF's light-directing capabilities and graphene's SPR effect produces extremely sensitive RI detection [9, 10]. These sensors have the capacity to detect a wide range of refractive indices, making them useful for a variety of applications [11, 12]. They have the potential to identify analytes without the use of extra labels or markers, which simplifies the testing procedure. These developments have the potential to improve a variety of applications, including the detection of biomolecules such as proteins and DNA for medical diagnostics and drug discovery [1, 13]. Monitoring pollutants and toxins in the air, water, and soil. Identifying and measuring particular chemicals used in industrial operations or food safety analysis [14]. To have a better understanding, the original study article you cited most likely delves into the following topics in depth: The graphene-functionalized PCF sensor was designed and fabricated using specific procedures [15, 16]. Characterization methods are used to assess sensor performance, such as sensitivity and detection range. Experimental findings demonstrate the sensor's capacity to detect RI variations in a variety of analytes [17]. A comparison with existing RI sensing technologies to illustrate the benefits of the proposed method. By continuing your research and reading the original publication, you will obtain a thorough grasp of graphene-functionalized PCFs' tremendous potential for next-generation RI sensing applications [18].

Based on the finite element method (FEM), the model in this study is made in the COMSOL environment. The PCF was surrounded by a layer of gold and reinforced with a layer of graphene to provide the sensor with high accuracy in RI variations and high sensitivity that enables the sensor to detect any small changes in the RI of the analyte. These are stable materials that are not affected by the passage of time. The gold layer was placed off-center to prevent reflections that could occur. The position of the graphene can be changed to obtain better properties.

2. Present Design

The proposed sensor consists of a large cylinder with a radius made of silica, where t is the gold thickness and 1.02 nm is the three-layer graphene thickness. The silica cylinder is surrounded by cylindrical layers of gold, and before it is graphene. Four circular holes in a cross section with a radius are made for the analyte and placed at angles and at a distance. Two sets of air holes are then placed, represented by rectangular cross-sections, where the outer set has rectangles with dimensions and is distanced from the center by distance, while the inner group has rectangles with dimensions and is distanced from the center by distance. The air holes and the inner surface of the gold can be coated—one or both of them—with a layer of graphene, depending on the researcher's vision. To avoid scattering and reflections, a perfectly matched layer (PML) of thickness surrounds the whole composition. Table 1 provides the values of the simulation's parameters, and the design of a typical sensor system configuration is shown in Figure 1. The design of a typical sensor system configuration is shown in Figure 2.

Edelweiss Applied Science and Technology
ISSN: 2576-8484
Vol. 8, No. 4: 1387-1401, 2024
DOI: 10.55214/25768484.v8i4.1513

Table 1.
Dimensions of the suggested model and simulation parameters.

Parameter	Value	Parameter	Value
R_1	6.5 μm	L_1	2.135 μm
R_2	5.5 μm	L_2	3.135 μm
R_3	0.5 μm	l_1, l_2	5 μm , 3 μm
R_4	4.5 μm	w	0.3 μm
t	(20-60)nm	Graphene thickness	1.02nm
E_F	(0.01-2)eV	n_a	1.34-1.55

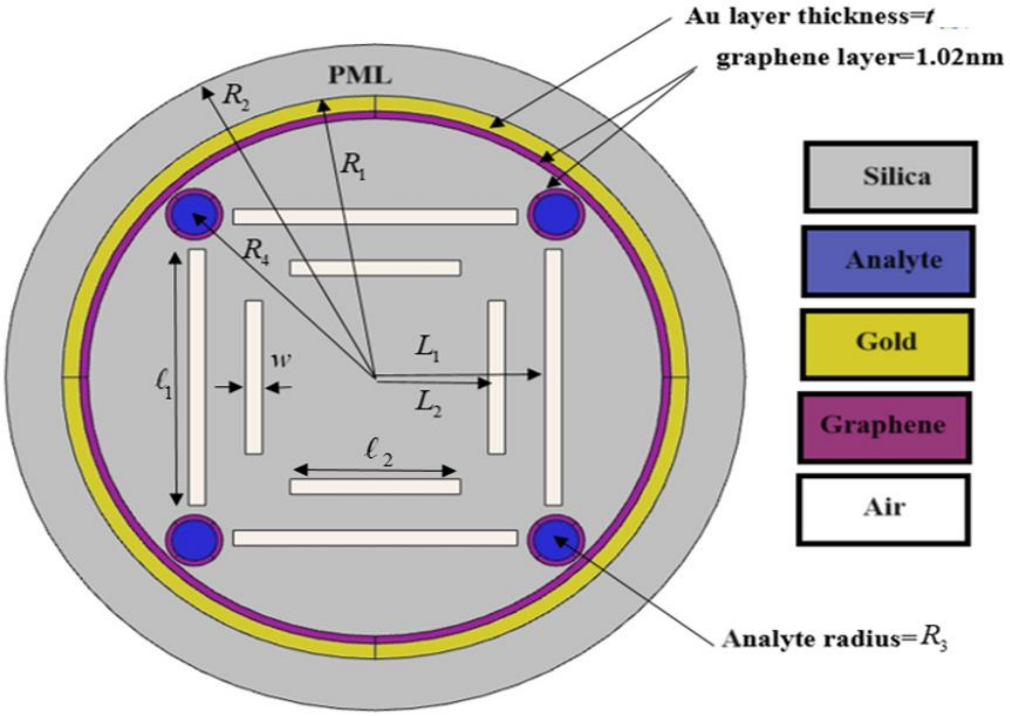

Figure 1.
The structure of the suggested model.

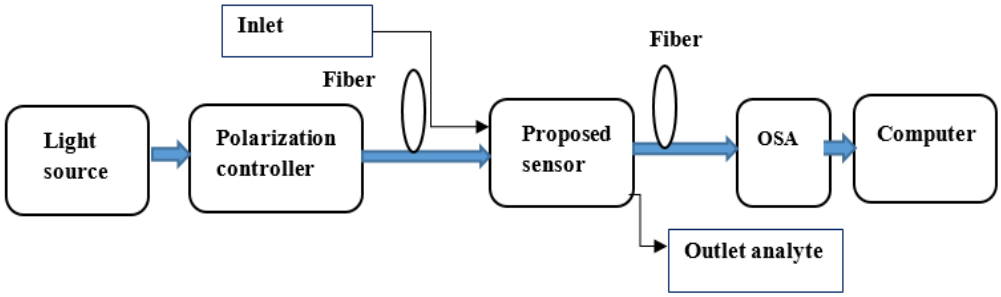

Figure 2.
Schematic representation of the usual sensing system configuration.

Edelweiss Applied Science and Technology
ISSN: 2576-8484
Vol. 8, No. 4: 1387-1401, 2024
DOI: 10.55214/25768484.v8i4.1513

3. Sensor Materials and Meters

There are five parts to the sensor: air, silica, gold, the sample, and the gold. We think that the RI of the air and sample stays the same even when the frequency changes, unless it changes very little because of changes in the silica, metal, and graphene media [4]. So, the rest of this article will only talk about the properties of gold, graphene, and silica's RI. The background of the sensor was made of fused silica glass, and the Sellmier equation [19] can be used to determine the dispersion parameters.

$$n_{sil} = \sqrt{1 + \sum_{j=1}^{3} \frac{A_j \lambda^2}{\lambda^2 - B_j}} \quad (1)$$

where $B_1 = 4.67914826 \times 10^{-3}\,\mu m^2, B_2 = 1.35120631 \times 10^{-2}\,\mu m^2, B_3 = 97.9340025\,\mu m^2,$ $A_1 = 0.6961663,$ $A_2 = 0.407942$, and $A_3 = 0.8974794$.

The way light moves through a general metallic medium is controlled by both bound and free electrons [20]. Interband transitions are basically quantum mechanical events [6]. They happen when a state below the Fermi level moves to a state above it that is not occupied. It turns out that only a few energy band transitions are important. These transitions are linked to critical points in the density of states that form at symmetry points in the Brillouin zone. These points are usually called Van Hove singularities [21]. Interband absorption and emission happen because there are a lot of states in these areas. This makes the visible range go from the top of the d-band to numbers just above the Fermi level in the conduction band [22]. Free carriers make intraband changes possible, which happen at low energies. In the conduction band, electrons are free and form an electron gas. Their long-range interactions are thought of as group oscillations at the plasma frequency of the system [5]. As explained in the Drude model [21], intraband changes happen when electrons are pushed to a higher energy level within the same band. This helps with free-electron infrared absorption. In this idea, the EM radiation coming in at the frequencies mentioned below is reflected by the electric field of the electrons in the metal screen. Because electrons can't process it quickly enough, higher-frequency electromagnetic radiation gets through [23]. The complex dielectric permittivity that goes with this has both the Drude component for the intraband effect and the Lorentz term for the interband transition. This is shown in the form of the Drude-Lorentz model [22].

$$\varepsilon_r(w) = 1 - \frac{w_p^2}{w^2 + i\gamma w} + \sum_i \frac{f_i w_i^2}{w_i^2 - w^2 - i\gamma_i w} \quad (2)$$

where i stands for the damping effect, the resonance frequencies, the resonant modes, and the weighting factors. It's important to note that noble metals usually have a lot of interband transitions because their bound electrons have different band layouts. We can see the best numbers for common metals in the Drude-Lorentz model in Table 2. In optoelectronic systems, these metals are used a lot. The experimental settings (like the shape and method of production) have a big effect on the readings of these optical data, so it's important to pick the right optical data.

Table 2.
Parameter values of gold for the Drude-Lorentz model [22].

Parameter	Value	Parameter	Value	Parameter	Value
f_o	0.760	γ_d	0.053	$w_1(eV)$	0.415
f_1	0.024	$\gamma_1(eV)$	0.241	w_2	0.830
f_2	0.010	γ_2	0.345	w_3	2.969
f_3	0.071	γ_3	0.870	w_4	4.304
f_4	0.601	γ_4	2.494	w_5	13.32
f_5	4.384	γ_5	2.214		

Edelweiss Applied Science and Technology
ISSN: 2576-8484
Vol. 8, No. 4: 1387-1401, 2024
DOI: 10.55214/25768484.v8i4.1513

It is feasible to improve the qualities of other materials by incorporating graphene, the most significant substance in the known world. The electrical conductivity of a single layer of graphene is defined as [24].

$$\sigma_{intra} = \frac{je^2 k_B T_o}{\pi\hbar^2 (w + 2j\Gamma)} \left[\frac{E_F}{k_B T_o} + 2\ln\left(1 + e^{-E_F / k_B T_o}\right) \right] \quad (3a)$$

$$\sigma_{inter} = \frac{je^2}{4\pi\hbar} \ln\left[\frac{2|E_F| - (w + 2j\Gamma)}{2|E_F| + (w + 2j\Gamma)} \right], k_B T_o \square E_F \quad (3b)$$

Where the total conductivity is. In the above equations, the chemical potential is the reduced Planck constant, the scattering rate is the carrier relaxation lifetime, the Boltzmann constant is the temperature, and the electron change is We consider tri-layer graphene to be present on the substrate for graphene sheets. As a result, the number of layers, which belongs to a few-layer graphene, can behave as a superposition of a single sheet. Furthermore, the effective thickness of a monolayer of graphene. The total thickness of graphene sheets is 25.. The formula below can be used to determine the permittivity of graphene in the mid-infrared frequency range [11].

$$\varepsilon_g = 1 + \frac{j\sigma(w)}{w\varepsilon_o t} \quad (4)$$

The success of a plasmonic sensor is judged by each parameter, and calculations are done using confinement loss for various RIs of the analyte. For measuring sensitivity, confinement loss is an important factor that can be shown using the method below: [12]

$$\alpha\left(\frac{dB}{cm}\right) = 8.868\, k_o Im\{n_{eff}\} \times 10^4 \quad (5)$$

Where α is the modal loss and $\mathrm{Im}\{n_{eff}\}$ is the imaginary component of effective RI in the fundamental mode. The structural factors used to design the sensor have a significant impact on its performance. For the PCF-SPR sensors, analyte detection happens when there are minute variations in the wavelength of the bio-targets in the surrounding environment. Consequently, one of the most important factors is spectral sensitivity S_λ, which is described as follows [25].

$$S_\lambda = \frac{\Delta\lambda_{peak}}{\Delta n_a} \left(\frac{nm}{RIU} \right) \quad (6)$$

Where $\Delta\lambda_{peak}$ refers to the resonance peak difference and Δn_a means the variations in two adjacent RIs of an analyte. This, $\Delta n_a = 0.01$ is taken in our simulation. Additionally, the resolution of the sensor is important since it indicates the degree to which the sensor can detect changes in the analyte RI. One can compute the sensor resolution by utilizing the following relationship [26].

$$R = \frac{\Delta n_a \Delta\lambda_{\min}}{\Delta\lambda_{\text{peak}}} (\text{RIU}) \quad (7)$$

where $\Delta\lambda_{\min} = 0.01nm$ and Δn_a represent the lowest spectral resolution and analyte RI difference, respectively.

4. Results and Discussion

We discussed a group of cases, such as the change in Fermi energy, the change in the site of graphene, the change in gold thickness, and others. The loss as a function of wavelength remains similar

Edelweiss Applied Science and Technology
ISSN: 2576-8484
Vol. 8, No. 4: 1387-1401, 2024
DOI: 10.55214/25768484.v8i4.1513

to Figure 3, with changes in the peak value and the shift of the resonant wavelength to the right or left. Therefore, we will not repeat shapes similar to this one because it would be useless elaboration.

Figure 3 shows the relationship between loss and wavelength for a wide range of RIs of analyte in the presence of a layer of graphene on gold and a Fermi energy of 0.5 *eV*. We notice from the figure that the loss increases until it reaches a peak and then decreases. The value of the peak decreases with the increase in RI of the analyte and at the same time, it is shifted to the right. Note that all curves meet at wavelength $3.65\,\mu m$. When light interacts with a graphene-gold layer, it causes a unique type of interaction termed resonance. Assume the material likes to absorb or scatter some wavelengths over others. Shorter, higher-energy wavelengths resonate more strongly with the material, resulting in increased light absorption or scattering. This loss peaks at a particular wavelength where the light-material interaction is highest. As the wavelength increases, the resonance lessens, and the amount of light lost decreases. An analyte with a higher RI suggests a more intense light-material interaction. However, this might be unexpected! A greater interaction reduces peak loss because the material interacts with all wavelengths of light rather than just the resonant wavelength. Interestingly, all analytes, regardless of refractive index, exhibit the same amount of light loss at a given wavelength of $3.65\,\mu m$. This points to a unique characteristic of the graphene-gold combination. It's as if there's a unique absorption or scattering mechanism built in that dominates at that specific wavelength, regardless of the analyte.

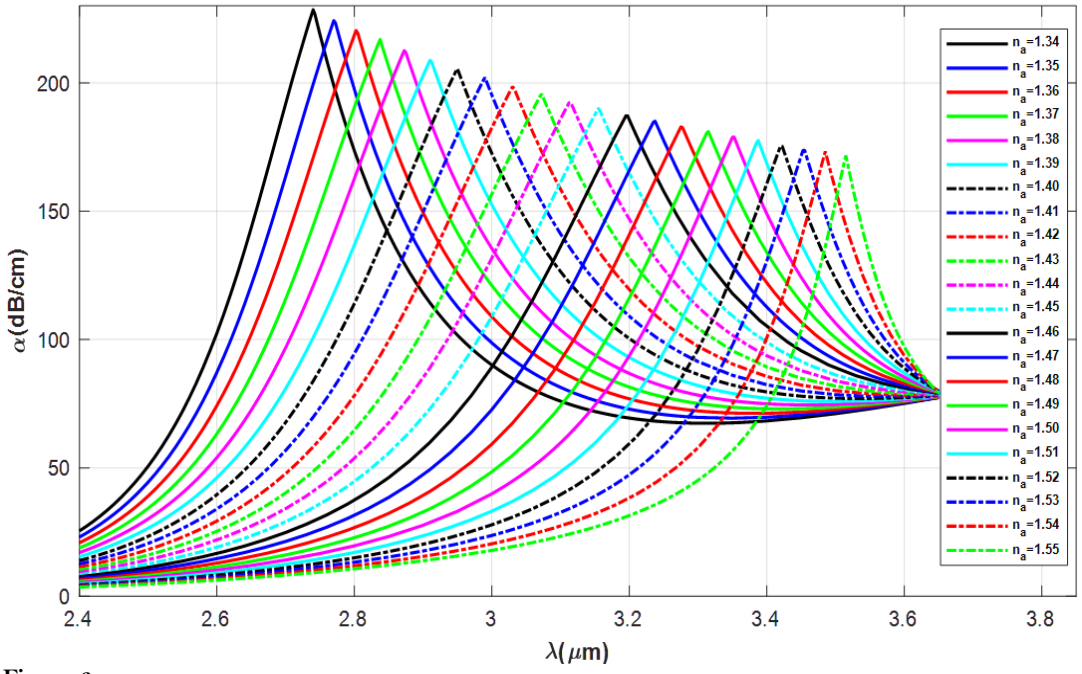

Figure 3.
The losses as functions of wavelengths for many RI of analyte with step index 0.01, where the graphene on gold at E_F =0.5*eV*.

Figure 4 represents the real refractive index as a function of wavelength for a selected set of RIs of the analyte. The graphene plasmonic PCF exhibits an unexpected increase in its real refractive index at a certain wavelength of light. Why is this happening? The secret resides in a phenomenon known as resonance. At this wavelength, the "electron traffic" in graphene and gold (known as plasmons) interacts intensely with light. This interaction is similar to traffic congestion, causing the light to be absorbed and bounce around more inside the fiber. The longer light passes through the fiber, the greater

Edelweiss Applied Science and Technology
ISSN: 2576-8484
Vol. 8, No. 4: 1387-1401, 2024
DOI: 10.55214/25768484.v8i4.1513

its refractive index. Graphene absorbs a large amount of infrared radiation, and its two-dimensional structure scatters it further. Additionally, the fiber's multilayer structure traps light, amplifying the plasmon effect. All of these elements combine to produce a dramatic increase in the refractive index at the resonant wavelength. This increase in the refractive index presents fascinating possibilities! It may be used to create improved sensors that detect minute changes in materials, high-speed communication devices that send data more quickly, and even more efficient solar cells that convert light into power. Scientists can even manipulate the refractive index by modifying the characteristics of graphene and the fiber itself. Figure 5 depicts the connection between resonance loss and RI of the analyte when graphene is positioned on gold and surrounding the analyte at E_F =0.1 *eV* and E_F =0.5 *eV*. The connection is perfectly linear when E_F =0.1 *eV*, but it deviates a little bit from the linearity property when the RI of analyte is larger for E_F =0.5 *eV*. At a higher Fermi energy, there might be a stronger interaction between the light and the electrons in graphene, leading to a more complex energy transfer process that's not simply dependent on the RI. The higher Fermi energy could alter the properties of the surface plasmons on the gold surface, affecting their sensitivity to the RI change.

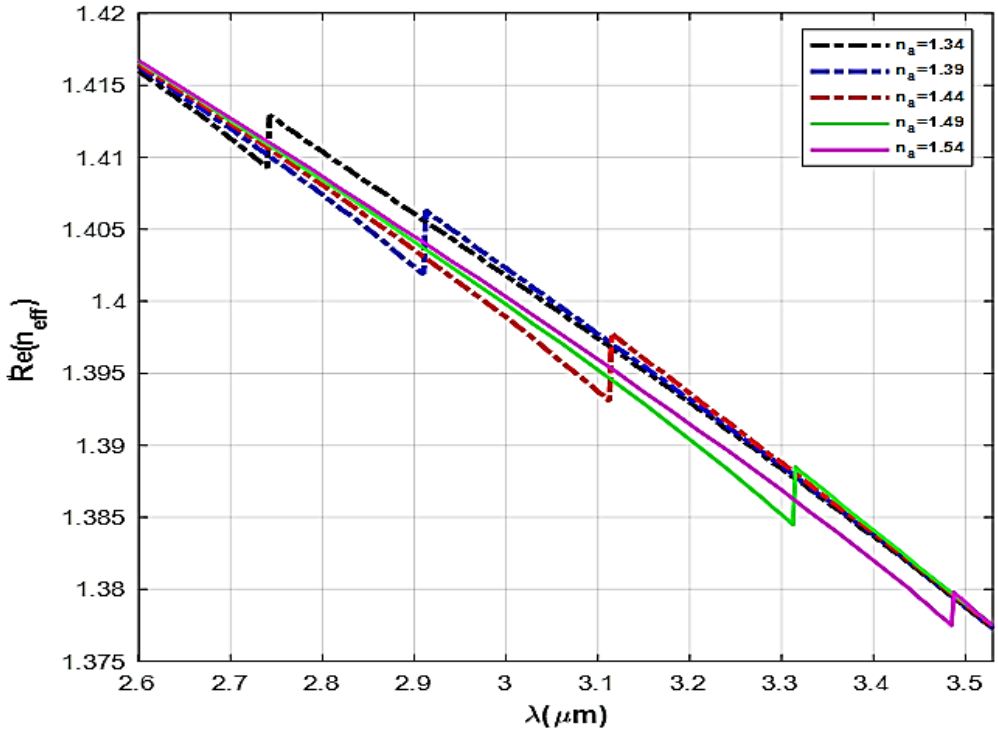

Figure 4.
The real part of effective refractive index as a function of wavelengths for selected RI of analyte, where the graphene on the gold at Ef=0.5*eV*.

Edelweiss Applied Science and Technology
ISSN: 2576-8484
Vol. 8, No. 4: 1387-1401, 2024
DOI: 10.55214/25768484.v8i4.1513

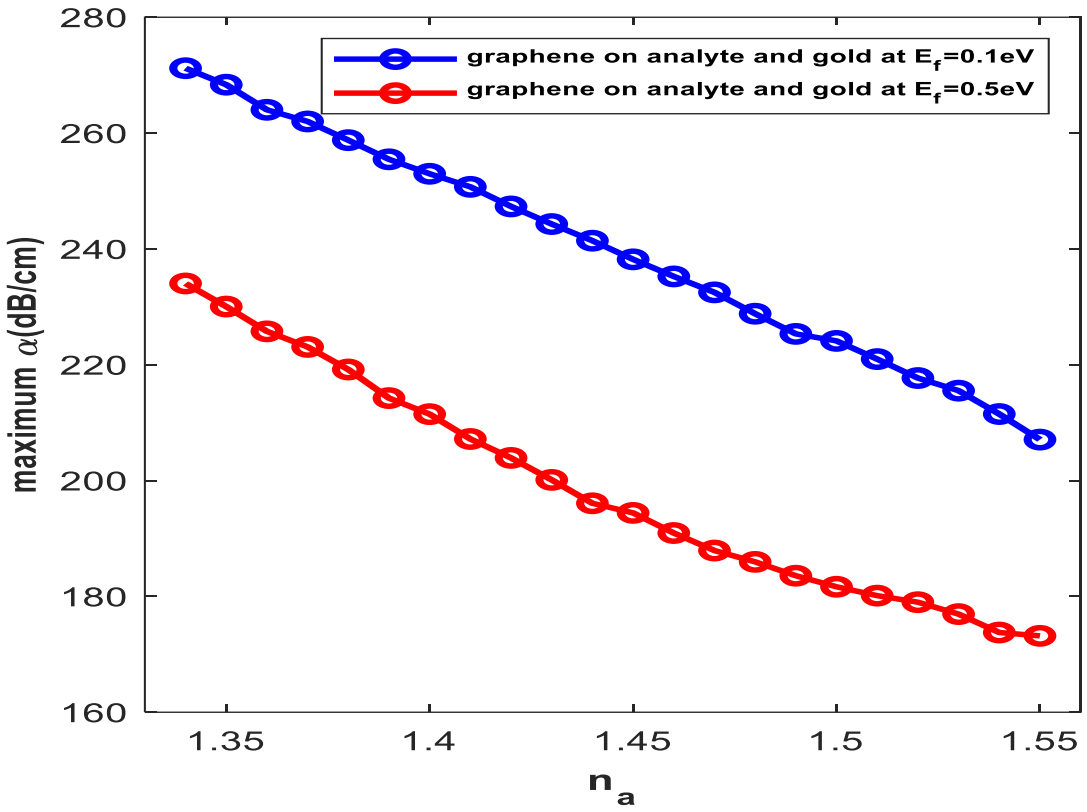

Figure 5.

The loss at resonance as functions of RI of analyte, where graphene on gold and analyte for E_F =0.1eV and 0.5eV.

Figure 6 shows a bar plot of spectrum sensitivity and sensor resolution based on the analyte RI, where graphene is on gold at E_F =0.5 eV. Notice that the spectral sensitivity grows from 3000 *nm/RIU* to 4250 *nm/RIU* as the analyte's RI increases, then declines to 3000 *nm/RIU* with considerable volatility in the spectral sensitivity values. This shows that a higher RI analyte improves the sensor's ability to detect light in a given wavelength band. This might be due to a shift in the interaction of light with surface plasmons (collective electron oscillations) in the graphene layer. A higher RI environment may boost the interaction between light and plasmons, resulting in a greater signal at specific wavelengths. The following decline and changes in sensitivity might be attributed to a variety of variables. It might imply a complicated interaction between the RI and other variables, such as light scattering or absorption inside the analyte and graphene layers. Also, the sensor resolution decreases from the value 3.4×10^{-5} *RIU* until it reaches 2.3×10^{-5} *RIU* and then returns to the same value as the RI of the analyte increases, with some fluctuations in the value of the sensor resolution. This noise might come from a variety of sources, including temperature fluctuations and shot noise inside the material. The improved resolution may indicate that the dominant noise source becomes less prominent at higher RI levels. The sensor resolution appears to drop from a higher value to a lower value before recovering as the RI increases. Resolution refers to the sensor's capacity to discern minor changes in the RI of the analyte. A loss in resolution might be attributed to increasing noise in the sensor's response at higher RI.

Edelweiss Applied Science and Technology
ISSN: 2576-8484
Vol. 8, No. 4: 1387-1401, 2024
DOI: 10.55214/25768484.v8i4.1513

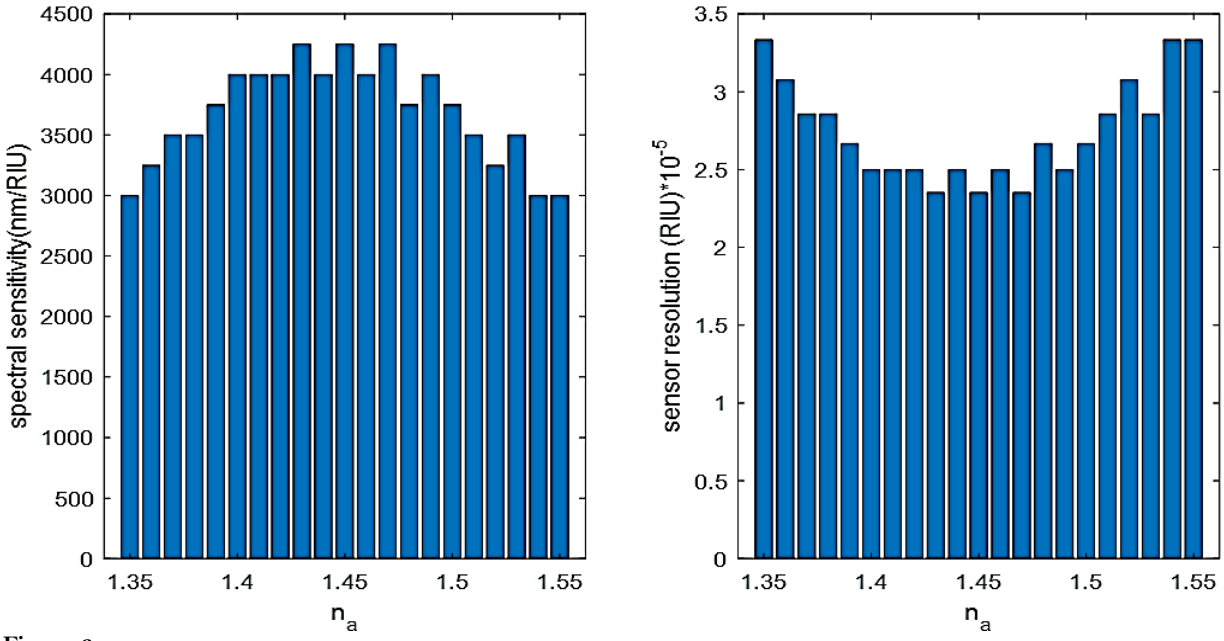

Figure 6.

The spectral sensitivity and sensor resolution as functions of RI of analyte, where the graphene on the gold at E_F =0.5*eV*.

Figure 7 depicts the resonant wavelength and maximum loss as functions of the RI of the analyte for a collection of graphene sites. The figure shows how graphene affects the interaction of light and an analyte. The resonant wavelength increases linearly as the RI of the analyte increases, with the maximum resonant wavelength occurring when there is no graphene and the lowest when graphene is present around the analyte. On the other hand, we notice that the maximum loss value drops as the RI of the analyte increases, and that it is highest in the absence of graphene and lowest when graphene is present around the analyte. The main takeaway is the plasmonic impact. Increasing the RI analyte improves the interaction between light and surface plasmons on graphene, resulting in a longer resonant wavelength for resonance. Without graphene, there is no plasmonic interaction, resulting in the maximum resonant wavelength. In contrast, graphene around the analyte provides a strong plasmonic interaction, resulting in the lowest resonant wavelength. The highest loss trend represents the plasmonic impact. It lowers as RI increases because light interacts with the analyte more efficiently, reducing energy loss due to plasmon excitation. In essence, the figure shows how graphene may be utilized to control the light-analyte interaction by changing the plasmonic response. This has potential uses in biosensors, where certain resonance wavelengths or maximum losses are required for effective detection. The linear relationship between the resonance wavelength and the RI of the analyte is important for several reasons: The linear relationship allows easy prediction of the resonant frequency for any value of n_a. They can be used to design sensors based on resonance frequency measurement to determine the n_a material. The linear relationship provides high accuracy in measuring n_a, reduces errors resulting from inaccurate measurement, facilitates the analysis of experimental data, helps to better understand the physical phenomena associated with resonance, and contributes to the development of new theories about the behavior of materials.

Edelweiss Applied Science and Technology
ISSN: 2576-8484
Vol. 8, No. 4: 1387-1401, 2024
DOI: 10.55214/25768484.v8i4.1513

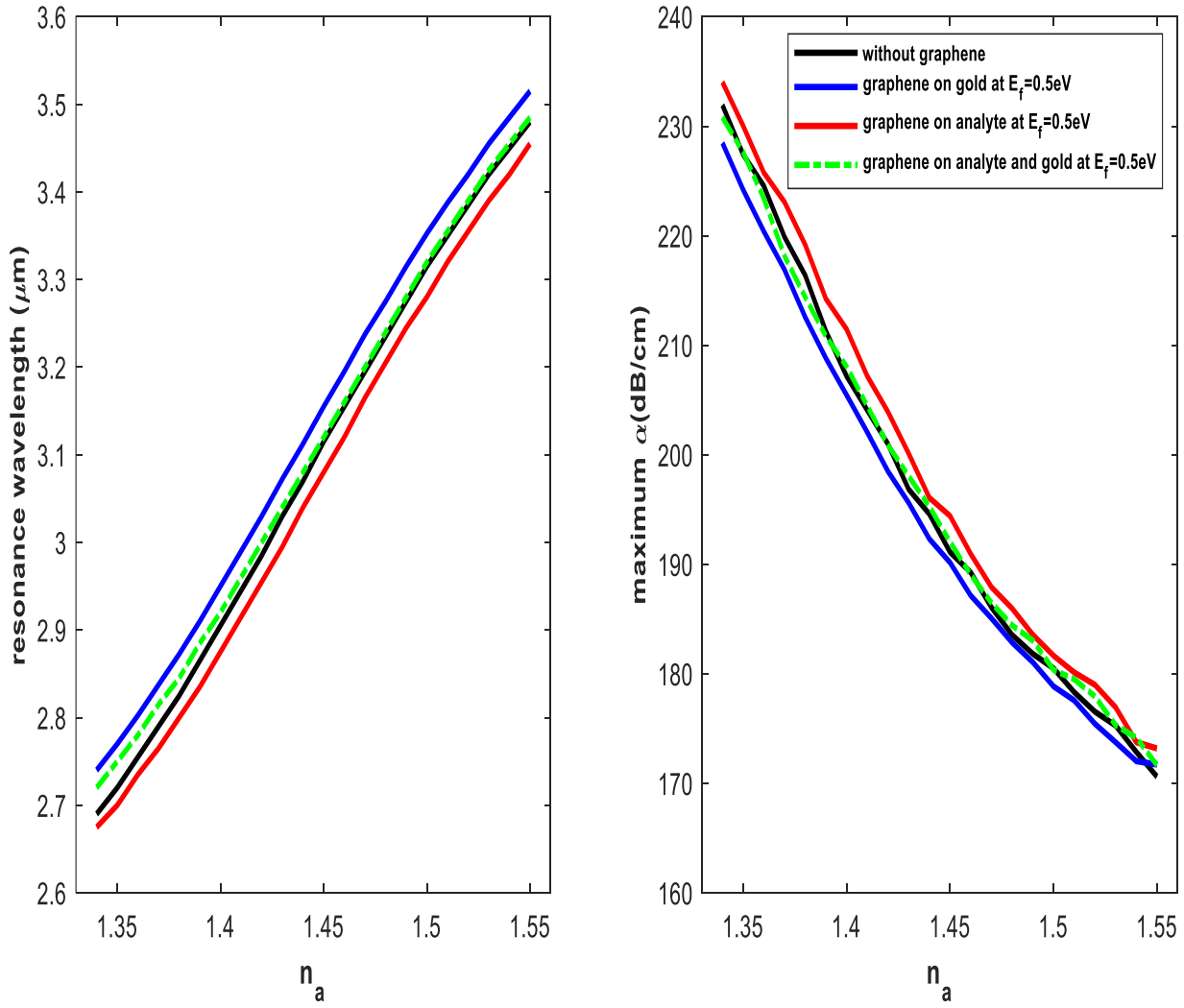

Figure. 7.
The resonance wavelength and maximum attenuation as functions of analyte refractive indices, for different locations of graphene at E_F =0.5eV.

Figure 8 represents a plot bar of the spectral sensitivity as a function of the RI of analyte for several graphene sites at Ef=0.5eV. It is clear from the figure that sensitivity is highest in the middle and decreases on the sides, with some variations. By calculating the sensitivity mean for all RIs of analyte, we see that the best case is the case in which graphene covers the analyte holes. Several graphene sites refer to various arrangements of graphene across the PCF. Covering the holes entirely may improve the light-matter interaction, resulting in a greater wavelength shift for RI changes. The particular position of graphene relative to the holes may alter the interaction of light and SPR, and therefore the sensitivity.

Edelweiss Applied Science and Technology
ISSN: 2576-8484
Vol. 8, No. 4: 1387-1401, 2024
DOI: 10.55214/25768484.v8i4.1513

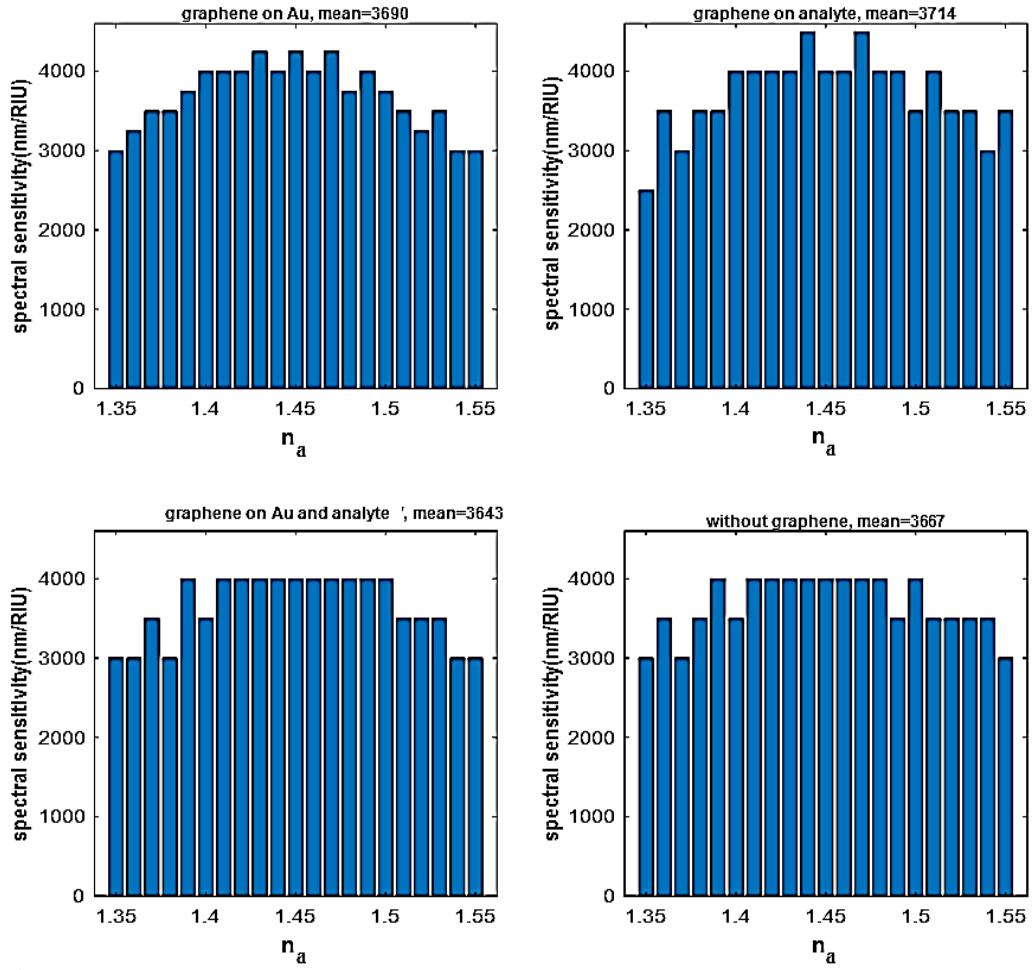

Figure 8.

The spectral sensitivity and as function of RI of analyte for different graphene sites at E_F =0.5eV.

Figure 9 shows a bar plot of sensor resolution based on analyte RI, using graphene on gold and analyte at $E_F = 0.1eV$ and E_F =0.5 *eV*. The figure shows that the case E_F =0.5 *eV* remains similar to the previous figure, but using a lower Fermi energy of 0.1 eV generally leads to a reduction in sensor resolution, where the median values are similar with slight increases at $n_a < 1.4$ and $n_a > 1.5$. Fermi energy, which determines how graphene interacts with electrons, impacts the sensor's resolution. Higher energy (E_F =0.5 *eV*) is anticipated to produce stronger surface plasmons (electron waves) that may differentiate between different RIs of the analyte, resulting in greater resolution. Poorer energy (E_F =0.1 *eV*) diminishes these plasmons, making it difficult to distinguish the RI of the analyte and resulting in poorer resolution. While there are certain difficulties at specific RI ranges, the figure establishes Fermi energy as an important component in improving sensor performance. Fig. 10 shows the resonance loss and resonance wavelength as functions of gold thickness for selected cases of RIs of analyte, where graphene on analyte and gold at E_F =0.5*eV*.

Edelweiss Applied Science and Technology
ISSN: 2576-8484
Vol. 8, No. 4: 1387-1401, 2024
DOI: 10.55214/25768484.v8i4.1513

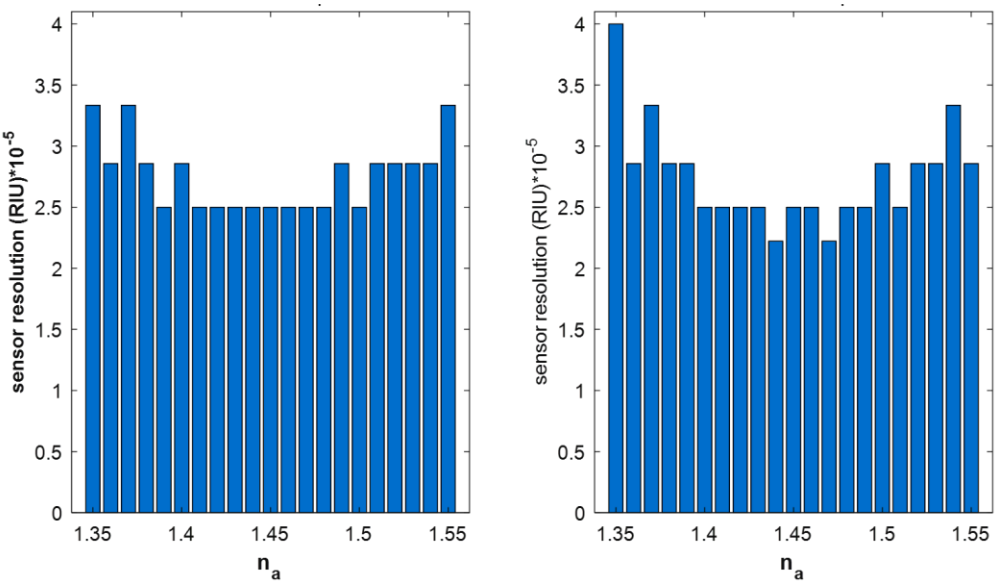

Figure 9.

The sensor resolution for E_F =0.1 and 0.5 eV, where graphene on gold and analyte.

In Figure 10, the resonance loss grows with the gold thickness until it reaches a peak, after which it drops until it reaches 200 dB/cm. The peak reached varies depending on the RI of the analyte, with the peak occurring at 29 nm, 26 nm, and 25 nm gold thicknesses, respectively. In turn, case n_a =1.37 has a peak value that jumps to reach 540 dB/cm. Light interacts with a metallic surface, causing electrons to collectively vibrate. The resonance varies based on the metal and surrounding medium. Thicker gold films first increase resonance loss due to increased light contact but eventually decrease when damping effects take over. The RI of the analyte effects peak resonance loss and appropriate gold thickness. An analyte with n_a =1.37 has a very significant peak loss, suggesting a strong light-plasmon interaction at that particular gold thickness. This interaction between gold thickness and solution characteristics enables SPR to be employed in sensing applications, where changes in the surrounding medium are recognized by monitoring resonance properties. Also, the figure represents the resonant wavelength as a function of gold thickness for a selected RI of the analyte. We note that the resonant wavelength decreases for all curves with increasing gold thickness. On the other hand, we note that the larger the RI of the analyte, the larger resonant wavelength. The seemingly conflicting behavior can be attributed to the complicated nature of light interaction with the metal surface. A thicker coating allows for greater light contact, but it also adds dampening effects. These dampening effects become more significant as thickness increases, causing resonance to occur at shorter wavelengths. The major point is that both gold thickness and solution RI affect the resonant wavelength in SPR. While a thicker layer appears to need a longer wavelength, the interaction with damping effects results in the opposite outcome.

Edelweiss Applied Science and Technology
ISSN: 2576-8484
Vol. 8, No. 4: 1387-1401, 2024
DOI: 10.55214/25768484.v8i4.1513

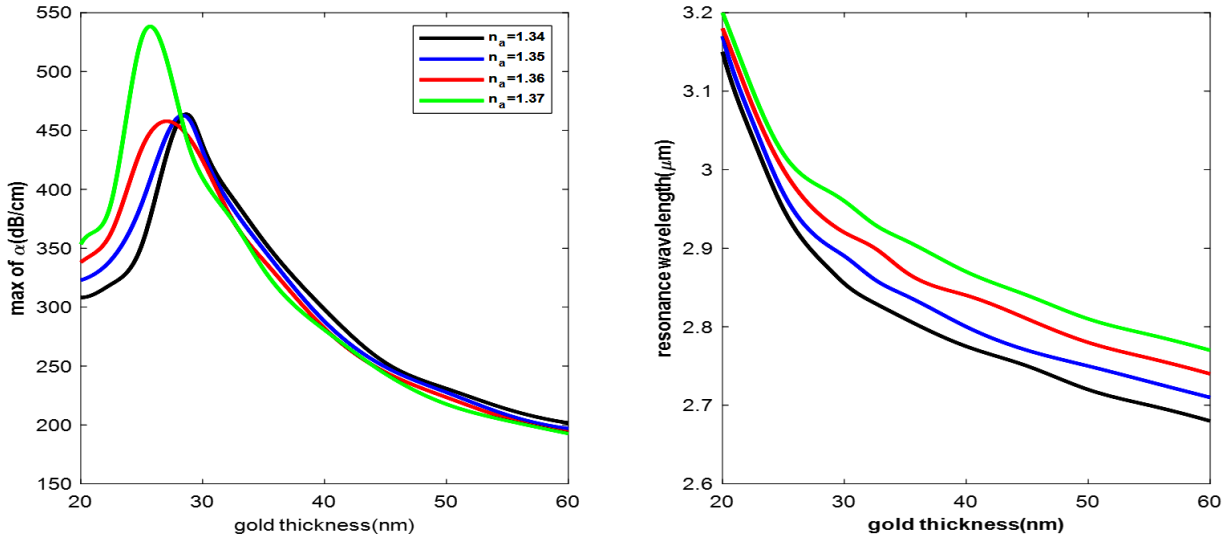

Figure 10.
The resonance loss and resonance wavelength as functions of gold thickness for many RIs of analyte, where graphene on analyte and gold at E_F =0.5 *eV*.

Figure 11 shows a plot bar of spectral sensitivity as a function of gold thickness for three cases of RI of the analyte, where the graphene is above the gold and around the analyte, and that E_F =0.5 *eV*. It is clearly evident from the figure that the gold thickness changes the spectral sensitivity depending on the RI of analyte used, as we find for case n_a =1.35 that the sensitivity starts from 2000 *nm/RIU* and reaches 3500 *nm/RIU* at gold thickness 30 *nm* and then returns to 2000 *nm/RIU* and then stabilizes almost at 3000*nm/RIU*. For the case n_a =1.36, we see that the sensitivity starts at 1000 *nm/RIU*, unstably reaches 4300 *nm/RIU* at the gold thickness of 43 nm and then declines to 3000 *nm/RIU*. For case n_a =1.37, we also see that the sensitivity starts at 2000 *nm/RIU*, increases unstably, reaches 4100 *nm/RIU* at a gold thickness of 37 *nm* and then returns to stability at 3000 *nm/RIU*. Accordingly, the gold thickness that best maximizes sensitivity can be chosen. The first increase in sensitivity with gold thickness can be attributed to a higher interaction of light with surface plasmons in a thicker layer. This can result in a bigger wavelength shift for RI changes. The peak and subsequent drop in sensitivity might be attributed to conflicting variables. As gold thickness grows, damping effects may become more pronounced, diminishing overall sensitivity. Furthermore, the interaction of light with graphene may get more complicated as thickness increases, influencing the total reaction. The dependency of optimum gold thickness on analyte RI implies that there exists a certain combination of gold film thickness and surrounding medium that maximizes the circumstances for a substantial wavelength shift as RI varies. Overall, the text outlines a complicated interplay between gold thickness, graphene presence, and analyte RI, which influences the system's spectrum sensitivity. While the particular process employing graphene is not explicitly stated, the dependency on these elements is consistent with the concepts of SPR and light-matter interaction.

Edelweiss Applied Science and Technology
ISSN: 2576-8484
Vol. 8, No. 4: 1387-1401, 2024
DOI: 10.55214/25768484.v8i4.1513

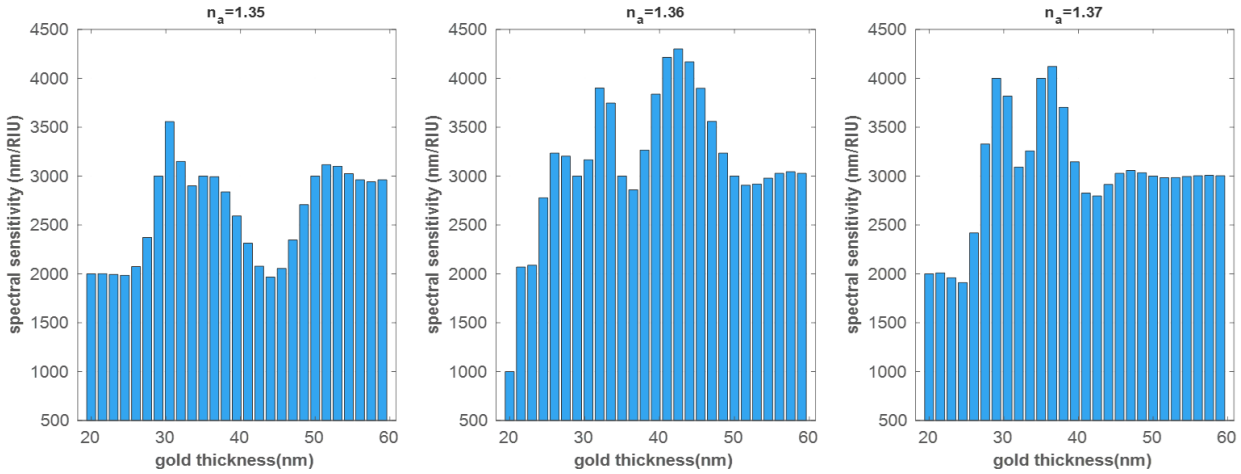

Figure 11.
The spectral sensitivity as functions of gold thickness for the indicated RI of analyte, where graphene on analyte and gold at E_F =0.5 *eV*.

5. Conclusions

In conclusion, the graphene-coated PCF sensor represents a viable method for very accurate RI measurement. Optimizing the sensor's design is critical for optimal performance. The higher Fermi energy in graphene provides improved precision for detecting minor RI changes. Graphene positioning has a major influence on the sensor's response, with the greatest plasmonic interaction happening when the graphene surrounds the analyte. The appropriate thickness within the PCF enhances light-material interaction and sensitivity. The appropriate thickness varies according to the material under consideration. The sensor's performance is dependent on the intricate interaction between light, graphene, and analyte. This relation determines parameters such as resonance wavelength, maximum loss, and spectral sensitivity. By carefully adjusting these parameters, the graphene-PCF sensor has the potential to become a very sensitive and adaptable instrument for RI measurements.

References

[1] Y. Zhan, Y. Li, Z. Wu, S. Hu, L. Li, X. Liu, J. Yu, Y. Huang, G. Jing, H. Lu, H. Guan, W. Qiu, J. Dong, W. Zhu, J. Tang, Y. Luo, J. Zhang and Z. Chen, "Surface plasmon resonance-based microfibre sensor with enhanced sensitivity by gold nanowires", *Optical Materials Express*, 8(12), 3927-3940, 2018. Available from https://doi.org/10.1364/OME.8.003927.

[2] T. Li, L. Zhu, X. Yang, X. Lou and L. Yu, "A refractive index sensor based on H-shaped photonic crystal fibers coated with Ag-graphene layers", *Sensors*, 20(3), 741, 2020. Available from https://doi:10.3390/s20030741.

[3] M. Salman, H. Muhammad and H. Yasser, "Effects of holes radius on plasmonic photonic crystal fiber sensor with internal gold layer", *Periodicals of Engineering and Natural Sciences*, vol. 8, pp.1288-1296, 2020. Available from http://dx.doi.org/10.21533/ pen.v8i3.1439.g613.

[4] A. Talib and H. Yasser. "Maximizing spectral sensitivity of plasmonic photonic crystal fiber sensor", *Optik International Journal for Light and Electron Optics* 249, 168228, 2022. Available from https://doi.org/10.1016/j.ijleo.2021.168228.

[5] H. Ali, H. Ammar, and H. Yasser, "Metal type effect on plasmonic fiber properties", *IOP Materials Science and Engineering* 928, 2020. https://doi.10.1088/1757-899X/928/7/072151.

[6] W. Zhang, J. Li and J. Xie, "High sensitivity refractive index sensor based on metamaterial absorber", *Progress In Electromagnetics Research M*, vol. 71, 107–115, 2018. Available from http://dx.doi. org/10.2528/PIERM18042903.

[7] H. Zhang, X. Zhou, X. Li, P. Gong, Y. Zhang and Y. Zhao, "Recent advancements of LSPR fiber-optic biosensing: combination methods, structure, and prospects", Biosensors, 13, 405, 2023. Available from https://doi.org/10.3390/bios13030405.
[8] G. Melwin and K. Senthilnathan, "High sensitive D-shaped photonic crystal fiber sensor with V-groove analyte channel", *Optik*, vo.213, 164779, 2020. Available from https://doi.org/10.1016/j.ijleo.2020.164779.
[9] M. Li, R. Singh, Y. Wang, C. Marques, B. Zhang and S. Kumar, "Advances in Novel Nanomaterial-Based Optical Fiber Biosensors: A Review", Biosensors, 12, 843, 2022. Available from https://doi.org/10.3390/ bios12100843.
[10] S. Fengen and H. Yasser, "Study of Soliton Interaction in Optical Fibers with Third Order Dispersion and Higher Order Nonlinear Effects", University of Thi-Qar Journal of Science , Vol. 10, No. 2, 2023.
[11] B. Li, T. Cheng, J. Chen, and X. Yan, "Graphene-enhanced surface plasmon resonance liquid refractive index sensor based on photonic crystal fiber", *Sensors*, vol. 19, p. 3666, 2019. Available from https://doi.org/10.3390/s19173666.
[12] M. Islam, A. Iftekher, K. Hasan, J. Nayen, S. Islam, Md. Khan, J. Chowdhury, F. Mehjabin, M. Islam, and Md. Islam, "Design and analysis of a biochemical sensor based on surface plasmon resonance with ultra-high sensitivity", *Plasmonics* 16(9), 2021. Available from https://doi.org/10.1007/s11468-020-01355-9.
[13] F. Zha, J. Li, P. Sun, and H. Ma, "Highly sensitive selectively coated D-shape photonic crystal fibers for surface plasmon resonance sensing", *Physics Letters A*, vol. 383, pp. 1825-1830, 2019. Available from https://doi.org/10.1016/j.physleta.2019 .02.046.
[14] M. Hasan, M. Rahman, K. Ahmed and M. Rana, "Design and analysis of a highly sensitive plasmonic photonic crystal fiber biosensor", *IEEE Access*, 8, 199202–199213, 2020. Available from https://doi.org/10.1016/j.optmat.2019.02.012.
[15] F. Zhenkai, "Surface plasmon resonance refractive index sensor based on photonic crystal fiber covering nano-ring gold film", Optical Fiber Technology 50: 194-199, 2019. Available from https://doi.org/10.1016/j.yofte.2019.03.018.
[16] M. Mahfuz, Md. Hasan, M. Momota, and S. Akter, "Asymmetrical photonic crystal fiber based plasmonic refractive index sensor". *Sensors*, vol. 19, p. 3794, 2019. Available from https://doi.org/10.1364/OSAC.2.001713.
[17] M. Mahfuz, M. Hossain, E. Haque, N. Hai, Y. Namihira, and F. Ahmed, "A bimetallic-coated, low propagation loss, photonic crystal fiber based plasmonic refractive index sensor", *Sensors*, vol.19, p.3794, 2019. Available from https://doi.org/10.3390/ s19173794.
[18] C. Wang, X. Zhang, H. Li, and Z. Liu, "Highly sensitive plasmonic photonic crystal fiber biosensor for label-free detection", *Optics Express*, 27(20), 28533-28544, 2019. Available from https://doi.org/10.1016/j.optmat.2019.02.012.
[19] G. Agrawal, "Nonlinear fiber optics", sixth edition, Academic Press, ch.2, pp.6-7, 2019. Available from https://doi.org/10. 1016/C2018-0-01168-8.
[20] H. Bahjat and H. Waried, "Study the synchronization for multiple transmitter- receiver nano quantum cascade lasers", University of Thi-Qar Journal of Science, Vol. 11 , No. 1 , 2024.
[21] S. Maier, "Plasmonics: fundamentals and applications", Springer Science and Business Media. 2007, ch.2-3, pp.5-35. Available from https://doi.org/10.1007/0-387-37825-1.
[22] M. Dresselhaus, "Solid-state physics," Lecture Notes, Part II; Optical Properties of Solids; Massachusetts Institute of Technology: Cambridge, MA, USA, Vol.17, 2001.
[23] R. Gangwar , A. Pathak, and S. Kumar, "Recent Progress in Photonic Crystal Devices and Their Applications: A Review", *Photonics*, 10, 1199, 2023. Available from https://doi.org/10.3390/photonics10111199.
[24] M. Rahman, S. Anower, L. Bashar and K. Rikta, "Sensitivity analysis of graphene coated surface plasmon resonance biosensors for biosensing applications", *Sens. Bio Sens. Res*, 16, 41–45, 2017. Available from https://doi.org/10.1016/j.sbsr.2017.11.001.
[25] V. Kumar, A. Kumar, D. Lee and S. Park, "Estimation of Number of Graphene Layers Using Different Methods: A Focused Review", *Materials*, 14, 4590, 2021. Available from https://doi.org/10.3390/ma14164590.
[26] J. Lou, T. Cheng, S. Li and X. Zhang, "Surface plasmon resonance photonic crystal fiber biosensor based on gold-graphene layers", *Opt. Fiber Technol*, 50, 206–211, 2019. Available from https://doi.org/10.1016/j.yofte.2019.03.028.

Edelweiss Applied Science and Technology
ISSN: 2576-8484
Vol. 8, No. 4: 1387-1401, 2024
DOI: 10.55214/25768484.v8i4.1513